DOI: 10.1002/chem.200700448

Controlled Growth of SnO_2 Hierarchical Nanostructures by a Multistep Thermal Vapor Deposition Process

Shuhui Sun,*[a] Guowen Meng,*[a] Gaixia Zhang,[b] Jean-Philippe Masse,[c] and Lide Zhang[a]

Abstract: Branched and sub-branched SnO_2 hierarchical architectures in which numerous aligned nanowires grew on the surface of nanobelt substrates have been obtained by a multistep thermal vapor deposition route. Branch size and morphology can be controlled by adjusting the temperature and duration of growth. The same approach was used to grow branched ZnO–SnO_2 heterojunction nanostructures. In addition, the third level of SnO_2 nanostructures was obtained by repeating the vapor deposition growth process. This technique provides a general, facile, and convenient approach for preparing even more complex nanoarchitectures, and should open up new opportunities for both fundamental research and applications, such as nanobelt-based three-dimensional nanodevices.

Keywords: crystal growth · electron microscopy · nanostructures · semiconductors · tin

Introduction

Quasi-one-dimensional (Q-1D) nanostructures (nanowires, nanorods, nanotubes, and nanobelts) have attracted a great deal of attention owing to their interesting geometries, unique properties, and novel potential applications in nanoscale devices.[1] A wide range of materials, including group IV,[2] III–V,[3] and II–VI semiconductors,[4] metals,[5] oxides,[6] and carbides,[7] have been prepared in the form of Q-1D nanostructures by a variety of methods. Once various 1D nanostructures have been synthesized, the next important step is to assemble them into electronic and photonic nanodevices,[8] which is a crucial step towards the realization of functional nanoscale systems.[9] Many novel structures, such as MgO fishbones,[10] novel SiO_x nanostructures,[11] ZnO nanonails[4c] and junction arrays,[12] and SnO nanoribbon networks,[13] have been synthesized. Hierarchical nanostructures in which the primary stems (or trunks) and branches consist of the same or different materials are an alternative for assembling 1D nanoscale building blocks into functional electronic devices. Hierarchical structures of various 1D nanoscale semiconductors, such as ZnO,[14a] In_2O_3,[14b] Si–SiO_2,[15] Pb–Se,[16] and ZnS[17] have been reported previously. In fact, these interesting nanostructures could be applied in field emission, photovoltaics, and supercapacitors. While much research has been devoted to the synthesis of hierarchical nanostructures, it still remains a great challenge to find a general synthetic scheme for formation of hierarchical nanostructures with well-controlled shape, size, and composition at different levels.

Here we present a multistep thermal vapor deposition route for the controlled growth of hierarchical nanohomo- and nanoheterojunctions, in which numerous aligned SnO_2 (or ZnO) nanowires or nanobelts have been grown on the surface of single-crystal SnO_2 nanobelt substrates. This method utilizes the catalyst-free vapor–solid (VS) growth mechanism for nanowires and nanobelts. Sequential growth of levels of nanowire and/or nanobelt "branches" by the VS process makes the complexity of such structures theoretically limitless, since each level (or generation) of branches can have different length, size, and chemical composition. This combination of technologies represents a significant step in the pursuit of functional nanoscale devices and nanomateri-

[a] Dr. S. Sun, Prof. G. Meng, Prof. L. Zhang
Key Laboratory of Materials Physics and
Anhui Key Laboratory of Nanomaterials and Nanostructures
Institute of Solid State Physics, Chinese Academy of Sciences
Hefei 230031 (China)
Fax: (+86) 551-559-1434
E-mail: shsuncn@hotmail.com
gwmeng@issp.ac.cn

[b] Dr. G. Zhang
Département de Génie Physique
École Polytechnique
Montréal H3C3A7 (Canada)

[c] Dr. J.-P. Masse
Centre de caractérisation microscopique des matériaux
École Polytechnique
Montréal H3C3A7 (Canada)

als, as the multistep procedure allows a level of control and flexibility not previously seen.[18] Hierarchical nanostructures of this type have multiple outlets and are ideal objects for the fabrication of nanoscale functional devices.[6a]

Results and Discussion

The substrate nanobelts and the second and third generations were synthesized in a horizontal high-temperature furnace, shown schematically in Figure 1a. A temperature gradient was thus established from the center to the end of the quartz tube, as shown in Figure 1b.

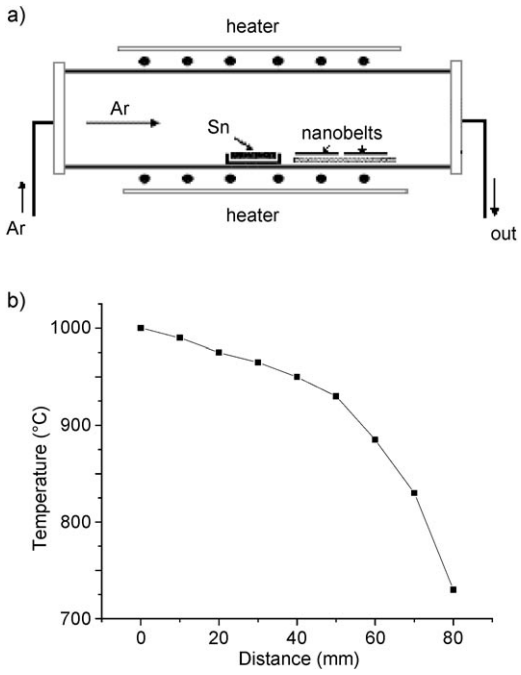

Figure 1. a) Schematic diagram of the horizontal furnace. b) Temperature distribution curve of the furnace.

The morphology of the products was examined by scanning electron microscopy (SEM). Figure 2a shows an SEM image of SnO_2 nanobelt substrates. The source heating temperature was increased to 1000 °C and the duration was extended to 4.5 h to increase the size of the nanobelt substrates, which is easy to control on the order of micrometers in width. The representative morphologies of the secondary SnO_2 nanostructures grown on SnO_2 primary nanobelts are revealed by field-emission (FE) SEM (see Figures 3 and 6 below).

The X-ray diffraction (XRD) pattern (Figure 2b) revealed the overall crystal structure and phase purity of the two as-synthesized products: bare nanobelt substrates (A), and nanobelts grown with nanowires (B). All the diffraction peaks for the two products match very well with those of tetragonal rutile SnO_2 ($a=4.738$, $c=3.187$ Å) obtained from

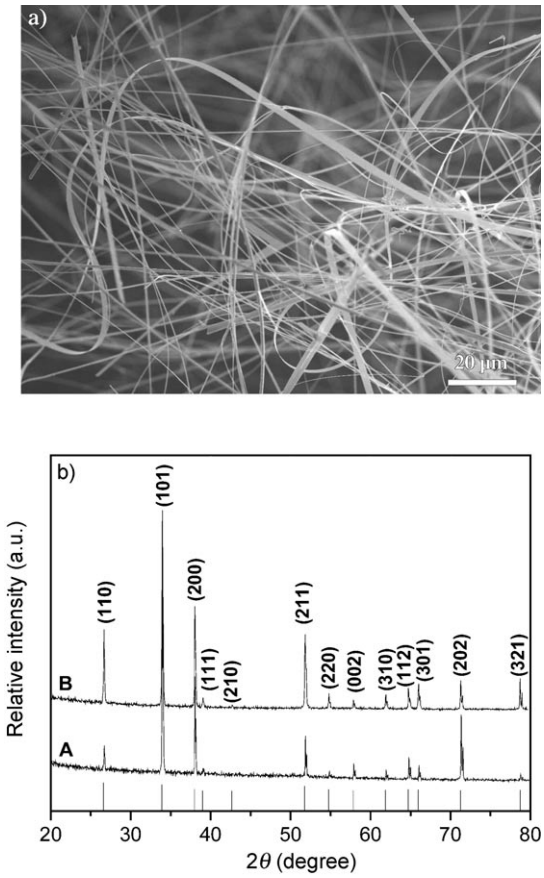

Figure 2. a) Typical SEM image of the as-grown SnO_2 nanobelts (to be used as the trunk or stem to grow secondary branches). b) XRD patterns recorded from the as-synthesized products: bare nanobelt substrate (A) and nanobelts grown with nanowires (B).

the JCPDS 41-1445 card, that is, the nanostructures consist predominantly of pure SnO_2.

For the hierarchical products synthesized in a substrate temperature zone of 830–850 °C for 1 h, the low-magnification SEM image in Figure 3a shows that well-aligned SnO_2 nanowire arrays with high density grew on the whole surface (top, bottom, and sides) of the primary nanobelt substrates, which still retain their beltlike morphology after secondary growth of nanowires. The magnified SEM image in Figure 3b reveals that the secondarily grown nanowires have lengths ranging from 10 to 20 μm and diameters of about 50 nm. The SnO_2 nanowires grown on the top and bottom (width dimension, indicated as "W" in the inset) surfaces of the nanobelts are well aligned in one direction on the substrates, whereas the nanowires on the side surface (thickness dimension, indicated as "T" in the inset) of the nanobelt grow predominantly in two directions on the substrate surface, which are found on almost all of the belts observed. The diameter of the secondary SnO_2 nanowires remains almost constant, except for the contact points with the nanobelt substrates, which are a bit thicker. The absence of catalyst tips at the end of the nanowires indicates a VS growth mechanism. Structural analysis of the branched nanostruc-

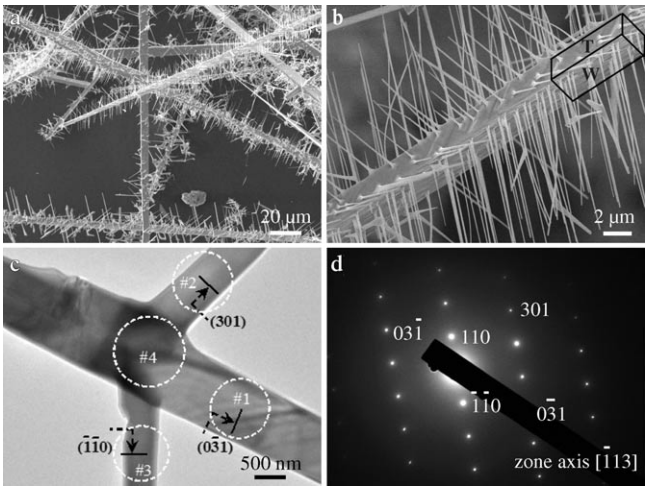

Figure 3. Typical SEM images of the as-synthesized product obtained at a substrate temperature of 830–850 °C after 1 h of growth. a) Low- and b) high-magnification images of SnO_2 hierarchical nanostructures. The inset shows a structural illustration of a nanobelt substrate in which the width and thickness dimensions of the nanobelt substrate are indicated by "W" and "T", respectively. c) Typical TEM image of the SnO_2 hierarchical nanostructure. d) The corresponding SAED pattern.

tures was performed by transmission electron microscopy (TEM). The low-magnification TEM image of an isolated branched SnO_2 nanostructure in Figure 3c reveals nanowires grown on the stem, in agreement with the results from SEM observations. The second-level nanowires could be broken off the stem by ultrasonic treatment during TEM sample preparation. Lattice-resolved HRTEM images were not obtained due to the slightly greater thickness of the selected regions. Interestingly, SAED patterns obtained from the different parts (marked by circles) of the branched nanostructure (backbone, junction, and branches) reveal similar reciprocal lattice peaks that suggest that the branched nanostructure is crystalline throughout the entire structure, as shown in Figure 3d. This can be indexed to be $[\bar{1}13]$ zone axis of the rutile-structured SnO_2 crystal. These results demonstrate that SnO_2 branches are epitaxial, and thus we expect these novel structures could yield interesting functional nanodevices.[19] The growth direction was obtained from analysis of the diffraction pattern by using the concept of the reciprocal lattice.

From the diffraction patterns, the lattice planes of $(0\bar{3}1)$, (301), and $(\bar{1}\bar{1}0)$, corresponding to stem and branches (Figure 3c), were obtained. The corresponding normal directions are $[h_1k_1l_1]=[0\bar{3}2.2]\approx[0\bar{3}2]$, $[h_2k_2l_2]=[302.2]\approx[302]$, and $[h_3k_3l_3]=[\bar{1}\bar{1}0]$, that is, the growth directions of the stem (#1) and the branches (#2 and #3) are $[0\bar{3}2]$, [302], and $[\bar{1}\bar{1}0]$, respectively. The stem-branching angles determined from the reciprocal lattice are 76.6° (branch #2) and 54° (branch #3). However, more detailed TEM characterization is necessary to elucidate the exact mechanism of branched nanostructure growth and the relationship between the orientation of the branches and the axis of the stem.

Elemental composition and purity of the product were studied by XPS analysis. The survey spectrum of the product (Figure 4a) indicates high purity of SnO_2, since only Sn- and O-related core levels are detectable, apart from a weak C 1s peak at about 285 eV. The presence of carbon is mainly due to exposure of the sample to air. High-resolution spectra of Sn $3d_{5/2}$ and O 1s are shown in Figure 4b and c, respectively. The Sn $3d_{5/2}$ peak, which shows a very symmetric line shape, is fitted by a single component with a binding energy of 486.6 eV and full width at half-maximum (FWHM) of 1.23 eV (similar to that of ca. 1.30 eV for pure SnO_2).[20] In addition, no peak corresponding to Sn^{2+} was detected, since its binding energy is typically downshifted from the Sn^{4+} peak by 0.7 eV.[20b] Thus, the deconvolution procedure confirmed the existence of only SnO_2. By contrast, the asymmetric O 1s peak is deconvoluted into three components, labeled as 1, 2, and 3, which are attributed as follows: O1 at 530.5 eV, Sn oxidation; O2 at 531.7 eV, C=O/C−OH; O3 at 533.0 eV, −COOH.[20c,21] The O2 and O3 peaks are mainly due to oxygenated carbon species on the SnO_2 surface when the sample was exposed to the atmosphere. We obtained a relative atomic concentration ratio O1:Sn of 1.93 for hierarchical nanostructures from the experimental XPS peak areas and their relative sensitivity factors, which indicates that the product is nothing but SnO_2.

Figure 5 shows a room-temperature photoluminescence (PL) spectrum of the SnO_2 hierarchical nanostructures. Two strong emission bands are centered at 432 and 539 nm. Since the energy gap of bulk SnO_2 is 3.62 eV (ca. 340 nm),[22] the two observed luminescence bands cannot be assigned to direct recombination of a conduction electron in the Sn 4d band with a hole in the O 2p valence band. Earlier reports indicated that 1D SnO_2 nanostructures exhibited broad luminescence bands between 400 and 600 nm.[23] We attribute the broad yellow band (540 nm) to oxygen vacancies, which are mainly located on the surface of the nanostructures and can form a series of metastable energy levels within the band gap of SnO_2 by trapping electrons from the valence band to make a contribution to the luminescence.[24] The origin of the blue-violet band (432 nm) probably is related to structural defects induced during growth.[17,25]

Reducing the growth duration from 1 h to 30 min leads to a decrease in the length of the secondarily grown nanowires, obtained in the same temperature zone (830–850 °C), to 3–6 μm, while the cross-array structures are maintained, as shown in Figure 6a. Furthermore, using a short growth duration (10 min) reveals that such an orientational relationship has already been established even in the initial growth stage (Figure 6b). The secondarily grown nanowires can be changed to nanobelts if the secondary growth temperature is increased. For example, with secondary growth parameters of 930 °C for 1 h rather than 830–850 °C for 1 h, arrays of nanobelts, rather than nanowires, with widths ranging from 100 to 300 nm grow on the substrate surface (Figure 6c). After a growth time of 3 h at 930 °C (Figure 6d), very long (up to hundreds of micrometers) nanobelts had grown on the whole surface of the primary nanobelt sub-

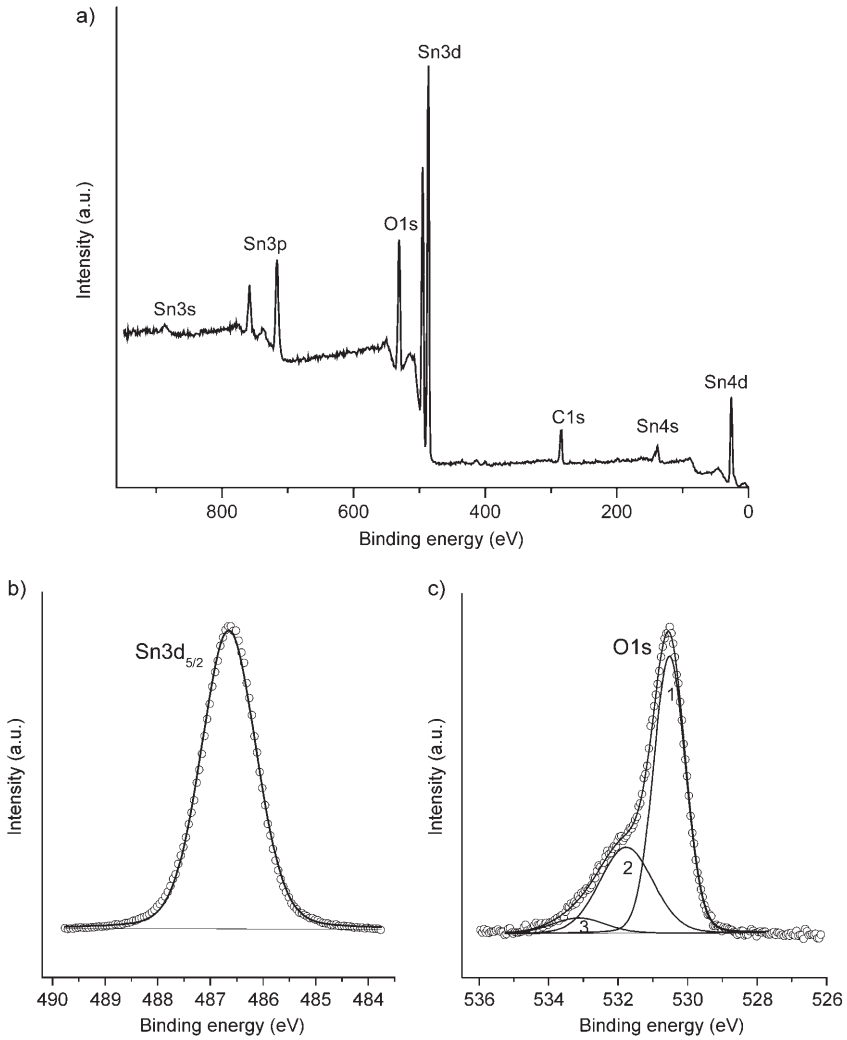

Figure 4. XPS spectra of SnO_2 hierarchical nanostructures. a) Survey spectrum. b) Sn $3d_{5/2}$ spectrum. c) C 1s spectrum. The adventitious C peak at about 285 eV was used to correct the binding-energy positions of the peaks. A Shirley background correction was applied to each spectrum before curve fitting. The peak sum of the fitted curves is represented by open circles.

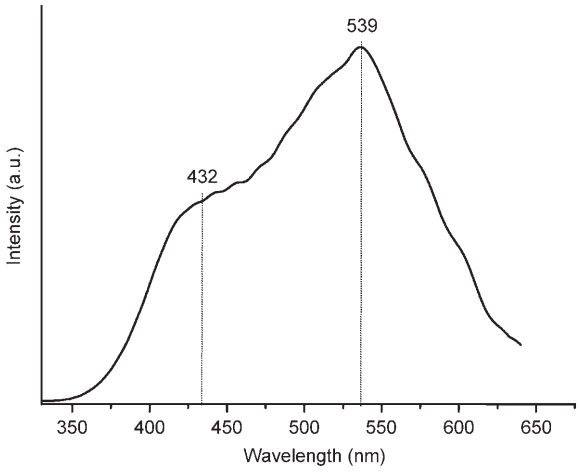

Figure 5. Room-temperature PL spectrum of SnO_2 hierarchical nanostructures.

strate (indicated by arrows in Figure 6d) with high density. The second level of SnO_2 nanobelts cross together, and the uniformity of the arrays is lost due to the greater flexibility of the longer nanobelts. The SEM results reveal no nanoparticles on any tips of the secondarily grown SnO_2 nanostructures. Because the only source material used in our synthesis was tin powder, it is likely that growth of secondary SnO_2 nanostructures is governed by the vapor–solid (VS) mechanism;[6a] that is, Sn vapor, evaporated from the starting material, oxidized, and deposited on the nanobelt substrate, acted as nucleation sites for the growth of SnO_2 nanostructures. It is generally believed that the growth temperature and gas-phase supersaturation determine the growth rate of surface planes and the final morphology of the crystals. The theoretical and most stable crystal habit of SnO_2 is tetragonal elongated along the *c* axis. Accordingly, SnO_2 nanostructures have optimized and secondary optimized growth directions. At higher temperatures and higher gas source concentrations, the single crystal grew along the two optimized directions simultaneously. Moreover, the growth along the optimized direction was faster than along the secondary optimized direction. Thus, SnO_2 nanobelts were formed. At lower temperatures and lower gas source concentrations, the single crystal grew along one of the two optimized directions to form SnO_2 nanowires. In this case, once the initial nucleation starts, the crystal grows in an epitaxial manner, which results in preferential orientation of SnO_2 lattice planes and finally formation of SnO_2 nanostructures.

Finally, we attempted to grow a third level of nanostructures, resembling sub-branches (marked by arrows in Figure 7). Again, the VS process works well for the growth of third-level of SnO_2 branches from the second-level branches. After three-step growth, branched nanowire/nanobelts resembling treelike nanostructures are formed. As can be seen in Figure 7, the third level contains far fewer nanowires, and this makes it difficult to carry out fourth-level growth. Possible reasons could include an effect of the size

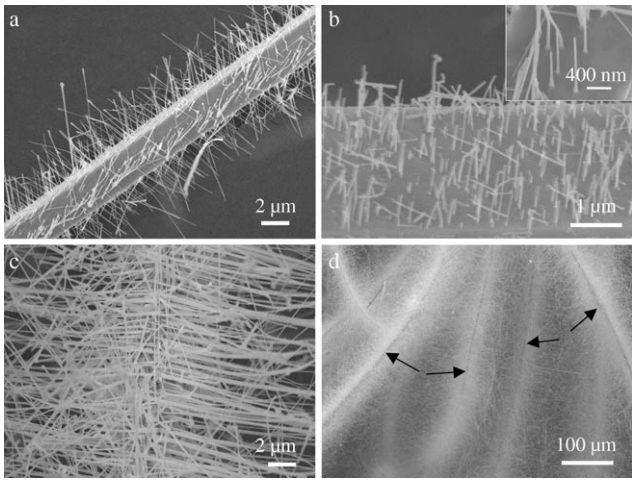

Figure 6. SEM images of SnO_2 hierarchical nanostructures synthesized with diverse experimental parameters. a) Nanowires grown on nanobelts for 30 min. b) Overall view of nanowires/nanorods grown on nanobelts for 10 min, and enlarged view of nanorods grown normal to the top surface of a nanobelt substrate (inset). c) Nanobelt arrays grown on the surface of the primary nanobelt substrate at 930 °C for 1 h. d) Overview of nanobelts grown on a substrate at 930 °C for 3 h; the arrows indicate the nanobelt stems.

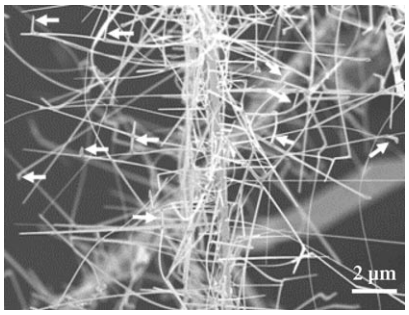

Figure 7. SEM image of an isolated three-level branched structure, with the third generation marked by arrows.

of the second-level substrate, a shadow effect, and so on. Although precise control over the position of the third generation on the second generation cannot be achieved, the density and morphology of the sub-branches could be controlled by varying the experimental parameters. Further work is underway.

The next step will be to incorporate different materials into the hierarchical nanostructures, by varying the composition of each level and within individual nanowires or nanobelts. Such hierarchical heterostructures will allow different device functionalities to be incorporated.[18] To illustrate this potential, we have grown ZnO nanoscale branches on SnO_2 nanobelt substrates (Figure 8), which will be described in detail elsewhere. These heteroarchitectures exhibit hierarchical structure, and the morphology can be modulated by changing the experimental parameters as well.

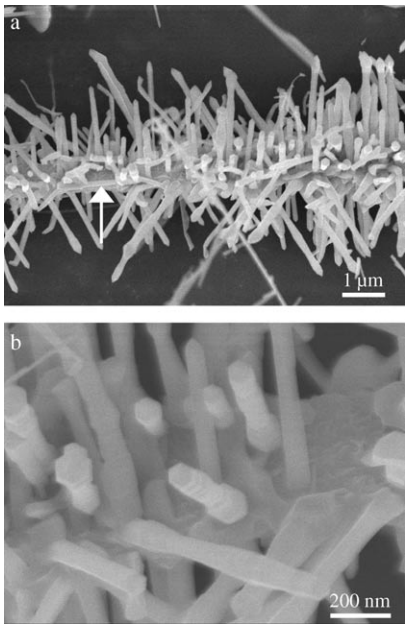

Figure 8. SEM images at two different magnifications of hierarchical heterostructures of ZnO nanowires grown on an SnO_2 nanobelt substrate.

Conclusion

In conclusion, we have reported the growth of well-aligned arrays of SnO_2 nanowires or nanobelts on micrometer-wide single-crystal SnO_2 primary nanobelt substrates by a multistep VS procedure. Our results offer a new route for the synthesis of nanobelt-based hierarchical nanostructures with attractive photoelectronic properties. The morphology and size of each level of branches could be controlled, and this provides great flexibility in the architectures. The ability to control the chemical composition makes it possible to grow hierarchical heterostructures. This unique class of nanobelt-based hierarchical nanostructures holds great potential for assembling electronics and photonics in three dimensions.

Experimental Section

Growth of the hierarchical SnO_2 nanostructures was performed in two steps. First, SnO_2 nanobelts were grown to serve as substrates (stems or trunks) on which nanowire or nanobelt branches were grown in the second step. Synthesis of the SnO_2 nanobelt substrates and epitaxial growth of nanowire and nanobelt branches were both performed in a quartz tube (inner diameter ca. 30 mm, length ca. 1200 mm) inserted into a horizontal high-temperature furnace. The process for the synthesis of single-crystal SnO_2 nanobelt substrates has been described in detail in our previous work.[26,19] In the present work, the heating temperature was increased to 1000 °C and the duration was extended to 4.5 h to increase nanobelt size to obtain micrometer-wide nanobelt substrates. The as-synthesized nanobelts had lengths of hundreds of micrometers, widths of hundreds of nanometers to micrometers, and thickness of 100–800 nm. For second-step growth, Sn powder (2 g, 200 mesh, purity >99 %) loaded in an alumina boat was placed in the central region of the quartz tube, as shown in Figure 1a. The tube was fed with argon at a flow rate of 100 sccm (standard cubic centimeters per minute). The temperature at the central region of the furnace was increased to 1000 °C at a rate of

15 °C min^{-1}, and then maintained at this temperature for 10 min to 3 h. A temperature gradient was thus established from the center to the end of the quartz tube, as shown in Figure 1b. The SnO_2 nanobelt substrates were placed at different temperature zones ranging from 930 to 800 °C along the downstream of the gas flow. The morphology and structure of the synthesized hierarchical nanostructures were characterized by field-emission scanning electron microscopy (FESEM, JEOL JSM 6700F) and transmission electron microscopy (TEM, Hitachi 800 operated at 200 kV). The photoluminescence (PL) spectrum was measured at room temperature with an Edinburgh luminescence spectrometer (FLS 920) using a xenon lamp (900) with a wavelength of 325 nm as excitation source. Ex situ X-ray photoelectron spectroscopic (XPS) analysis was carried out in a VG ESCALAB 220iXL, using a monochromated $Al_{K\alpha}$ source (1486.6 eV) at a base pressure of $< 10^{-10}$ Torr. High-resolution spectra were obtained at a perpendicular take-off angle with a pass energy of 20 eV and 0.05 eV steps. The instrument resolution was about 0.26 eV. All the binding energies were calibrated by the C 1s line of adventitious hydrocarbon at 284.8 eV.[20,27]

After Shirley background removal, the component peaks were separated by using the XPS Peak Fitting Program version 4.1.[21,28]

Acknowledgements

This work was supported by the National Science Fund for Distinguished Young Scholars (Grant No. 50525207), the Natural Science Foundation of China (Grant No. 10374092), and the National Basic Research Program of China (Grant No. 2007CB936601).

[1] a) P. G. Collins, A. Zettl, H. Bando, A. Thess, R. E. Smalley, *Science* **1997**, *278*, 100–103; b) Z. L. Wang, *Adv. Mater.* **2000**, *12*, 1295–1298; c) A. Modi, N. Koratkar, E. Lass, B. Wei, P. M. Ajayan, *Nature* **2003**, *424*, 171–174; d) J. T. Hu, T. W. Odom, C. M. Lieber, *Acc. Chem. Res.* **1999**, *32*, 435–445; e) *Nanowires and Nanobelts, Vol. II: Nanowires and Nanobelts of Functional Materials* (Ed.: Z. L. Wang), Kluwer Academic, New York, **2003**.

[2] a) A. M. Morales, C. M. Lieber, *Science* **1998**, *279*, 208–211; b) D. W. Wang, H. J. Dai, *Angew. Chem.* **2002**, *114*, 4977–4980; *Angew. Chem. Int. Ed.* **2002**, *41*, 4783–4786; c) J. D. Holmes, K. P. Johnston, R. C. Doty, B. A. Korgel, *Science* **2000**, *287*, 1471–1473; d) Y. Wu, P. Yang, *Chem. Mater.* **2000**, *12*, 605–607.

[3] a) X. F. Feng, C. M. Lieber, *Adv. Mater*, **2000**, *12*. 298–302; b) X. H. Chen, J. Xu, R. M. Wang, D. P. Wang, *Adv. Mater.* **2004**, *16*, 419–421; c) W. S. Shi, Y. F. Zheng, N. Wang, C. S. Lee, S. T. Lee, *Adv. Mater.* **2001**, *13*, 591–594; d) G. S. Cheng, L. D. Zhang, Y. Zhu, G. T. Fei, L. Li, C. M. Mo, Y. Q. Yong, *Appl. Phys. Lett.* **1999**, *75*, 2455–2457.

[4] a) Y. Li, G. W. Meng, L. D Zhang, F. Phillipp, *Appl. Phys. Lett.* **2000**, *76*, 201–203; b) P. X. Gao, Y. Ding, Z. L. Wang, *Nano Lett.* **2003**, *3*, 1315–1320; c) J. Y. Lao, J. Y. Huang, D. Z. Wang, Z. F. Ren, *Nano Lett.* **2003**, *3*, 235–238.

[5] a) Y. W. Wang, L. D. Zhang, G. W. Meng, C. H. Liang, G. Z. Wang, S. H. Sun, *Chem. Commun.* **2001**, *24*, 2632–2633; b) F. Favier, E. G. Walter, M. P. Zach, T. Benter, R. M. Penner, *Science* **2001**, *293*, 2227–2231.

[6] a) Z. W. Pan, Z. R. Dai, Z. L. Wang, *Science* 2001, 291, 1947–1949; b) R. Fang, Y. Y. Wu, D. Y. Li, M. Yue, A. Majumdar, P. D. Yang, *J. Am. Chem. Soc.* **2003**, *125*, 5254–5255; c) Q. Wei, G. W. Meng, X. H. An, Y. F. Hao, L. D. Zhang, *Nanotechnology* **2005**, *16*, 2561–2566.

[7] a) H. J. Dai, E. W. Wong, Y. Z. Lu, S. S. Fan, C. M. Liber, *Nature* **1995**, *375*, 769–772; b) T. H. Yang, C. H. Chen, A. Chatterjee, H. Y. Li, J. T. Lo, C. T. Wu, K. H. Chen, L. C. Chen, *Chem. Phys. Lett.* **2003**, *379*, 155–161.

[8] a) Y. Cui, C. M. Liber, *Science* **2001**, *291*, 851–853; b) Z. Y. Tang, N. A. Kotov, M. Giersig, *Science* **2002**, *297*, 237–240.

[9] Y. Y. Wu, H. Q. Yan, M. Huang, B. Messer, J. H. Song, P. D. Yang, *Chem. Eur. J.* **2002**, *8*, 1260–1268.

[10] Y. Q. Zhu, W. K. Hsu, W. Z. Zhou, M. Terrones, H. W. Kroto, D. R. M. Walton, *Chem. Phys. Lett.* **2001**, *347*, 337–343.

[11] a) Z. W. Pan, Z. R. Dai, C. Ma, Z. L. Wang, *J. Am. Chem. Soc.* **2002**, *124*, 1817–1822; b) S. H. Sun, G. W. Meng, M. G. Zhang, Y. F. Hao, X. R. Zhang, L. D. Zhang, *J. Phys. Chem. B* **2003**, *107*, 13029–13032.

[12] T. Gao, T. H. Wang, *J. Nanosci. Nanotechnol.* **2005**, *9*, 1120–1124.

[13] Z. L. Wang, Z. W. Pan, *Adv. Mater.* **2002**, *14*, 1029–1032.

[14] a) J. Y. Lao, J. G. Wen, Z. F. Ren, *Nano Lett.* **2002**, *2*, 1287–1291; b) J. G. Wen, J. Y. Lao, D. Z. Wang, T. M. Kyaw, Y. L. Foo, Z. F. Ren, *Chem. Phys. Lett.* **2003**, *372*, 717–722.

[15] a) C. H. Ye, L. D. Zhang, X. S. Fang, Y. H. Wang, P. Yan, J. W. Zhao, *Adv. Mater.* **2004**, *16*, 1019–1023; b) J. Q. Hu, Y. Bando, J. H. Zhan, X. L. Yuan, T. Sekiguchi, D. Golberg, *Adv. Mater.* **2005**, *17*, 971–975.

[16] B. Poudel, W. Z. Wang, D. Z. Wang, J. Y. Huang, Z. F. Ren, *J. Nanosci. Nanotechnol.* **2006**, *6*, 1050–1053.

[17] Y. Jiang, W. J. Zhang, J. S. Jie, X. M. Meng, J. A. Zapien, S. T. Lee, *Adv. Mater.* **2006**, *18*, 1527–1532.

[18] K. A. Dick, K. Deppert, M. W. Larsson, T. Martensson, W. Seifert, L. R. Wallenberg, L. Samuelson, C. M. Lieber, *Nano Lett.* **2004**, *4* 871–874.

[19] D. L. Wang, F. Qian, C. Yang, Z. H. Zhong, C. M. Lieber, *Nano Lett.* **2004**, *4*, 871–874.

[20] a) W. J. Song, S. K. So, D. Y. Wang, Y. Qiu, L. L. Cao, *Appl. Surf. Sci.* **2001**, *177*, 158–164; b) J. Szuber, G. Czempik, R. Larciprete, D. Koziej, B. Adamowicz, *Thin Solid Films* **2001**, *391*, 198–203; c) http://srdata.nist.gov/xps.

[21] a) M. Kwoka, L. Ottaviano, M. Passacantando, S. Santucci, G. Czempik, J. Szuber, *Thin Solid Films* **2005**, *490*, 36–42; b) D.-Q. Yang, E. Sacher, *J. Phys. Chem. B* **2005**, *109*, 19329–19334.

[22] a) A. Aoki, H. Sasakura, *Jpn. J. Appl. Phys.* **1970**, *9*, 582–582; b) C. Tatsuyama, S. Ichimura, *Jpn. J. Appl. Phys.* **1976**, *15*, 843–847.

[23] a) J. Q. Hu, X. L. Ma, N. G. Shang, Z. Y. Xie, N. B. Song, C. S. Lee, S. T. Lee, *J. Phys. Chem. B* **2002**, *106*, 3823–3826; b) J. Q. Hu, Y. Bando, Q. L. Liu, D. Golberg, *Adv. Funct. Mater.* **2003**, *13*, 493–496; c) G. Faglia, C. Baratto, G. Sberveglieri, M. Zha, A. Zappettini, *Appl. Phys. Lett.* **2005**, *86*, 011923–011925; d) S. H. Luo, J. Y. Fan, W. L. Liu, M. Zhang, Z. T. Song, C. L. Lin, X. L. Wu, P. L. Chu, *Nanotechnology* **2006**, *17*, 1695–1699.

[24] L. S. Huang, L. Pu, Y. Shi, R. Zhang, B. X. Gu, Y. W. Du, *Appl. Phys. Lett.* **2005**, *87*, 163124–163126.

[25] T. W. Kim, D. U. Lee, Y. S. Yoon, *J. Appl. Phys.* **2000**, *88*, 3759–3761.

[26] a) S. H. Sun, G. W. Meng, Y. W. Wang, T. Gao, M. G. Zhang, Y. T. Tian, X. S. Peng, L. D. Zhang, *Appl. Phys. A*, **2003**, *76*, 287–289; b) S. H. Sun, G. W. Meng, G. X. Zhang, T. Gao, B. Y. Geng, L. D. Zhang, J. Zuo, *Chem. Phys. Lett.* **2003**, *376*, 103–107.

[27] J. F. Moulder, W. F. Stickle, P. E. Sobol, K. D. Bomben, *Handbook of X-ray Photoelectron Spectroscopy* (Ed: J. Chastain), Perkin-Elmer Corp., MN, **1992**.

[28] http://www.phy.cuhk.edu.hk/≈surface/XPSPEAK/.

Received: March 22, 2007
Published online: August 3, 2007

